AAAS
Research
Volume 2020, Article ID 9398285, 11 pages
https://doi.org/10.34133/2020/9398285

Research Article

Ionic Liquid-Modified Porous Organometallic Polymers as Efficient and Selective Photocatalysts for Visible-Light-Driven CO_2 Reduction

Zhi-Hua Zhou, Kai-Hong Chen, Song Gao, Zhi-Wen Yang, and Liang-Nian He

State Key Laboratory and Institute of Elemento-Organic Chemistry, College of Chemistry, Nankai University, Tianjin 300071, China

Correspondence should be addressed to Liang-Nian He; heln@nankai.edu.cn

Received 25 June 2020; Accepted 31 August 2020; Published 25 September 2020

In the photoreduction of CO_2 to CO, the competitive H_2 evolution is always inevitable due to the approximate reduction potentials of H^+/H_2 and CO_2/CO, which results in poor selectivity for CO production. Herein, imidazolium-type ionic liquid- (IL-) modified rhenium bipyridine-based porous organometallic polymers (Re-POMP-IL) were designed as efficient and selective photocatalysts for visible-light CO_2 photoreduction to CO based on the affinity of IL with CO_2. Photoreduction studies demonstrated that CO_2 photoreduction promoted by Re-POMP-IL functioning as the catalyst exhibits excellent CO selectivity up to 95.5% and generate 40.1 mmol CO/g of Re-POMP-IL1.0 (obtained by providing equivalent [(5,5′-divinyl-2,2′-bipyridine)$Re(CO)_3Cl$] and 3-ethyl-1-vinyl-1*H*-imidazol-3-ium bromide) at 12 h, outperforming that attained with the corresponding Re-POMP analogue without IL, which highlights the crucial role of IL. Notably, CO_2 adsorption, light harvesting, and transfer of photogenerated charges as key steps for CO_2RR were studied by employing POMPs modified with different amounts of IL as photocatalysts, among which the CO_2 affinity as an important factor for POMPs catalyzed CO_2 reduction is revealed. Overall, this work provides a practical pathway to improve the CO_2 photoreduction efficiency and CO selectivity by employing IL as a regulator.

1. Introduction

Visible-light-driven reduction of CO_2 to fuel and/or chemicals provides a promising solution to solve both the environmental problems and the increased energy requirements [1–5]. As a typical product of CO_2 reduction reaction (CO_2RR), carbon monoxide (CO) is especially valuable in chemical industry because of its usage as the feedstock for a variety of carbon-based fuels [6, 7]. For photoreduction of CO_2 to CO, a proton source is always involved, producing the competitive H_2 evolution accompanied with the CO generation. In fact, the H_2 formation derived from protons trapping electrons is more favorable than the CO production from CO_2RR by comparing their reduction potentials [3]. Therefore, the development of photocatalysts capable of disfavouring the H_2 evolution in an attempt to enhance the efficiency and CO selectivity in CO_2RR is urgently needed.

For CO_2 photoreduction to CO, rhenium complexes of *fac*-[Re^I(N^N)$(CO)_3$X] (N^N=diimine, X=Cl, Br) as photocatalysts have gained long-term attention because of their excellent performance [8–16]. However, the notorious instability of *fac*-[Re^I(N^N)$(CO)_3$X] deriving form bimetallic decomposition greatly limits their application. Porous organic polymers (POPs), a type of polymer porous materials with micropores and/or mesopores formed by covalent bonds of organic structural units, feature with advantages of good chemical stability and easily tailored structures [17–20]. To date, several rhenium-metalated conjugated microporous polymers have been designed and demonstrated to be stable photocatalysts for CO_2 photoreduction [21–25]. Even though, the reported Re(I)-metalated porous materials, commonly fabricated by post modification, namely, polypyridine linkers are firstly constructed and then coordinate with $Re(CO)_5Cl$ [21–25]. Unfortunately, with post modification, incomplete coordination and random metal anchoring are difficult to avoid [26], resulting in compromised catalytic performance and/or inevitable H_2 evolution in most cases. Comparatively, direct polymerization of

metal complexes to prepare porous organometallic polymers (POMPs) can maximally maintain the structures of molecular catalysts, meanwhile, ensure uniform dispersion of metal sites in the porous matrix [26]. On the other hand, as the photocatalysts for CO_2RR, characteristics with good CO_2 adsorption, remarkable light-harvesting property, and efficient separation of photogenerated electrons and holes will be desirable [27]. However, it will be a time-consuming work to design an efficient photocatalyst for CO_2RR, because there is no panacea to meet all of these features. Hence, locating the key factors to CO_2RR will be helpful to solve this problem.

Ionic liquids (ILs), composed of cations and anions, have been widely applied in CO_2 capture and conversion [28–33]. For facilitated CO_2 absorption, IL has been directly added into the photocatalytic CO_2 systems, which are proven to accelerate the process of CO_2 to CO conversion and inhibits H_2 generation [34, 35]. In addition, the ionic group on the second coordination sphere, i.e., ionic second coordination sphere, has been proven to be promoting CO_2 photoreduction [16]. Therefore, we speculate ILs as regulators that can be covalently introduced into porous materials to enhance their photocatalytic performance.

Herein, the novel IL-modified Re-based POMP (Re-POMP-IL) through the simple and scalable copolymerization of Re bipyridine complex and IL was designed and synthesized as shown in Figure 1. By revealing the performance by employing Re-POMP-IL as the photocatalyst for CO_2 reduction to CO, the promoting effect of IL on photocatalytic activity and CO selectivity is highlighted. In addition, the influence of CO_2 adsorption ability, optical property, and lifetime for photogenerated charges on the performance of these polymers in photocatalytic CO_2RR was systematically evaluated by tuning the amount of IL in the preparation of Re-POMP-IL, in which the important factor of efficiency enhancement ascribed to the easy CO_2 adsorption of Re-POMP-IL was exposed.

2. Results

As shown in Figure 1, Re-based polymers used in this work can be easily prepared through the solvothermal copolymerization of [(5,5′-divinyl-2,2′-bipyridine)Re(CO)$_3$Cl] (**1a**) and 3-ethyl-1-vinyl-1*H*-imidazol-3-ium bromide (**2a**). For Re-POMP-IL1.0, an equivalent **1a** and **2a** were used. For comparison, Re-POMP without IL moiety was also synthesized by self-polymerization of **1a**. The synthesized polymers, attained as yellow solids, are stable in air and insoluble in water and organic solvents (e.g., CH_3CN). The chemical structures of Re-POMP and Re-POMP-IL1.0 were characterized by FT-IR and solid-state ^{13}C CP/MAS NMR technique. As exhibited in Figure 2(a), signals between 2025 and 1870 cm^{-1} are ascribed to the stretching vibration of CO ligand coordinated with Re(I). Compared with Re-POMP, the occurrence of the new peak at 1157 cm^{-1} in the FT-IR spectrum of Re-POMP-IL1.0 arises from the C-N bond vibration of covalently linked **2a**. In the solid-state ^{13}C CP/MAS NMR spectra (Figure 2(b)), chemical shifts ranging from 154 to 123 ppm indicate the signals of bipyridyl moieties, and the disappearance of signals of vinyl groups accompanying with the appearance of a new peak at 39 ppm demonstrates the successful polymerization of monomers [36]. The other peaks at 58, 46, 32, 18, and 15 ppm are assigned to the carbons of alkyl chains of polymerized **2a**. Similar morphologies of Re-POMP and Re-POMP-IL1.0 were observed by scanning electron microscopy (SEM) (Figure S4, see Supplementary Materials) and transmission electron microscopy (TEM) (Figure S4, see Supplementary Materials) measurements, which indicates the addition of IL unit does not affect the morphology of Re-POMP. The thermal stability of Re-POMP and Re-POMP-IL1.0 was measured through thermogravimetric analysis (TGA), and no obvious weight loss was found until temperature was above 300°C (Figure S5, see Supplementary Materials). Additionally, power X-ray diffraction (PXRD) pattern of Re-POMP-IL1.0 exhibits the broad diffraction peak (Figure S6, see Supplementary Materials), revealing the amorphous character of the polymer.

Subsequently, the elemental compositions of Re-POMP and Re-POMP-IL1.0 were identified by X-ray photoelectron spectroscopy (XPS). As shown in Figure 2(c), elements including C, N, O, Cl, and Re exist in the survey spectrum of Re-POMP. For Re-POMP-IL1.0, element of Br is also detected because of the introduction of **2a**. The high-resolution Re 4f spectra display two peaks belonging to Re $4f_{5/2}$ and Re $4f_{7/2}$, respectively (Figure 2(d)). Similar chemical environment of Re in **1a**, Re-POMP and Re-POMP-IL1.0 was observed, indicating that the polymerization does not destroy the coordination of Re(I) complex. Compared with Re-POMP, both of Re 4f peaks shift to lower binding energies for Re-POMP-IL1.0, indicating the increased Re electron density after the installation of IL. The high electron density on Re atom may facilitate the interaction between Re and CO_2 (vide infra). The accurate metal loading in polymers was further measured by inductively coupled plasma-optical emission spectroscopy (ICP-OES), and the Re contents of 31.0 and 24.4 wt% in Re-POMP and Re-POMP-IL1.0 were detected, respectively, which are basically consistent with the theoretical results. It is noteworthy that this is the highest Re content detected among the reported Re-based porous materials used in CO_2RR [21–25] (Table fS1, see Supplementary Materials), and such high concentrations of bpy-Re were conceived to dramatically improve their activity in CO_2 photoreduction.

The pore structures of polymers were investigated via N_2 physical sorption at 77 K. As exhibited in Figures 3(a) and 3(b), the N_2 adsorption/desorption isotherms of Re-POMP and Re-POMP-IL1.0 showed similar characteristics with a combination of type I and type IV patterns [37] with predominant pore sizes ranging from 0.5 to 10 nm, indicating their hierarchical porosity with micro- and mesopores. In fact, hierarchical porous polymers have remarkable advantages over those with microporous structures, profiting from the existence of mesopores facilitates the mass transfer process [17]. Porosity parameters of Re-POMP and Re-POMP-IL1.0 are summarized in Table 1, the Brunauer–Emmett–Teller (BET) surface areas are 452 and 326 $m^2 \cdot g^{-1}$, respectively, and total pore volumes are 0.33 and 0.24 $cm^3 \cdot g^{-1}$, respectively. Clearly, the introduction of **2a**

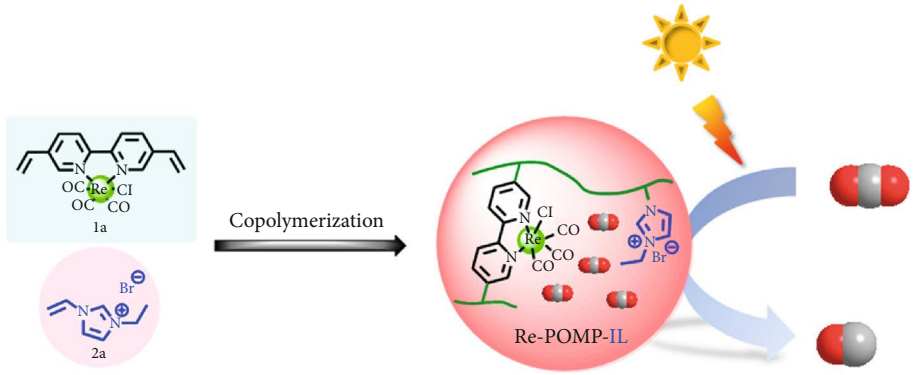

Figure 1: The IL-modified Re-based POMP for CO_2 photoreduction to CO.

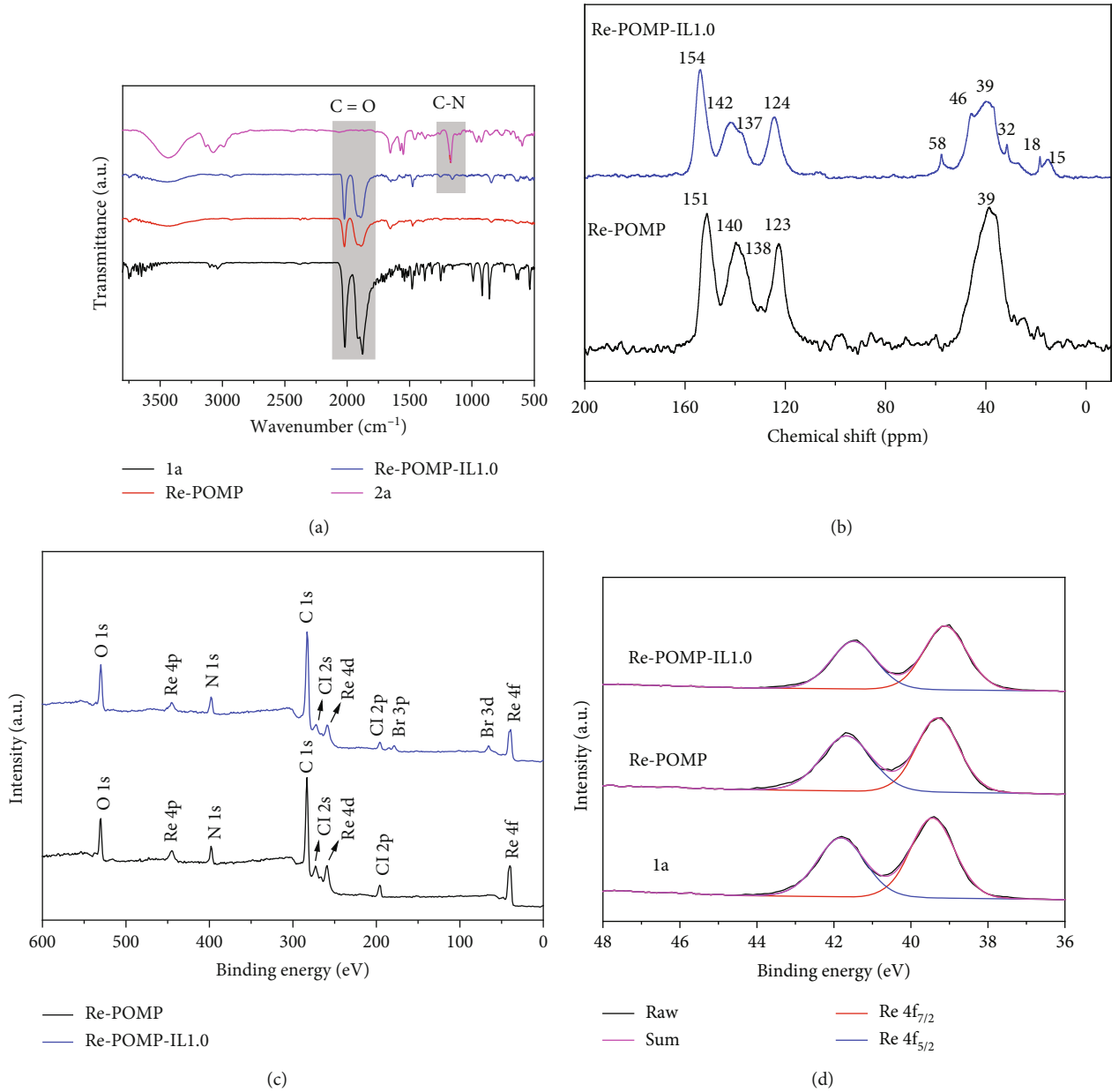

Figure 2: (a) FT-IR spectra of Re-POMP, Re-POMP-IL1.0, and their precursors. (b) Solid-state ^{13}C CP/MAS NMR spectra of Re-POMP and Re-POMP-IL1.0. (c) XPS survey spectra of Re-POMP and Re-POMP-IL1.0. (d) XPS spectra of Re 4f in 1a, Re-POMP, and Re-POMP-IL1.0.

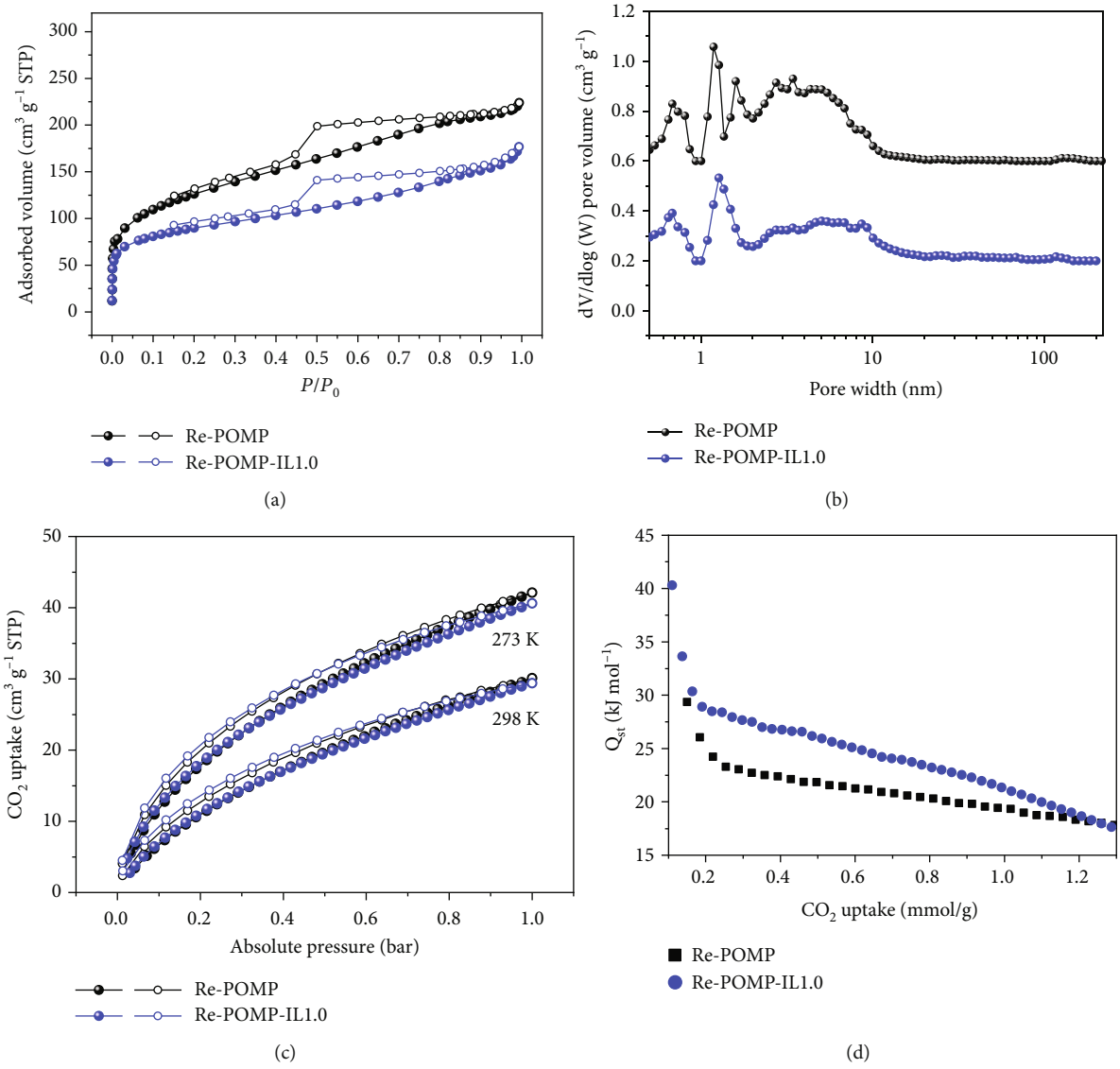

Figure 3: (a) Nitrogen sorption isotherms collected at 77 K. (b) Pore size distributions calculated by NLDFT. (c) CO_2 uptakes at 273 and 298 K. (d) Isosteric heat of adsorption (Q_{st}) plots for CO_2.

Table 1: Porosity properties, CO_2 uptake capacities, and lifetimes of excited states.

Polymers	S_{BET} ($m^2 \cdot g^{-1}$)[a]	V_{total} ($cm^3 \cdot g^{-1}$)[b]	CO_2 uptake ($cm^3 \cdot g^{-1}$)[c]		Q_{st} ($kJ \cdot Mol^{-1}$)[d]	τ_a (ns)[e]
			273 K	298 K		
Re-POMP	452	0.33	42.1	30.1	29.3	80
Re-POMP-IL1.0	326	0.24	40.6	29.4	40.3	93

[a]Specific surface area calculated by using the BET method. [b]Single point adsorption total pore volume at $P/P_0 = 0.95$. [c]CO_2 uptake capacities at 1 bar. [d]Isosteric heat of adsorption for CO_2. [e]The average photoluminescence lifetime of the polymer.

leads to the decrease in BET surface area and total pore volume, possibly due to the blocking of intrinsic pores by flexible chains or Br^- of IL [38].

The CO_2 uptake capacities of Re-POMP and Re-POMP-IL1.0 were also examined (Figure 3(c) and Table 1). A slightly reduced adsorption capacity of Re-POMP-IL1.0 relative to Re-POMP was observed, probably owing to the obvious reduced BET surface area and total pore volume after the introduction of IL. The interaction between polymers and CO_2 was further evaluated by using the Clausius–Clapeyron equation to calculate the isosteric heat of adsorption (Q_{st}). As described in Figure 3(d) and Table 1, Q_{st} values of Re-POMP and Re-POMP-IL1.0 are 29.3 and 40.3 $kJ \cdot mol^{-1}$, respectively, demonstrating the high CO_2 affinity of the synthesized polymers. Typically, the larger Q_{st} value of Re-POMP-IL1.0 than Re-POMP means the easier CO_2 capture, likely

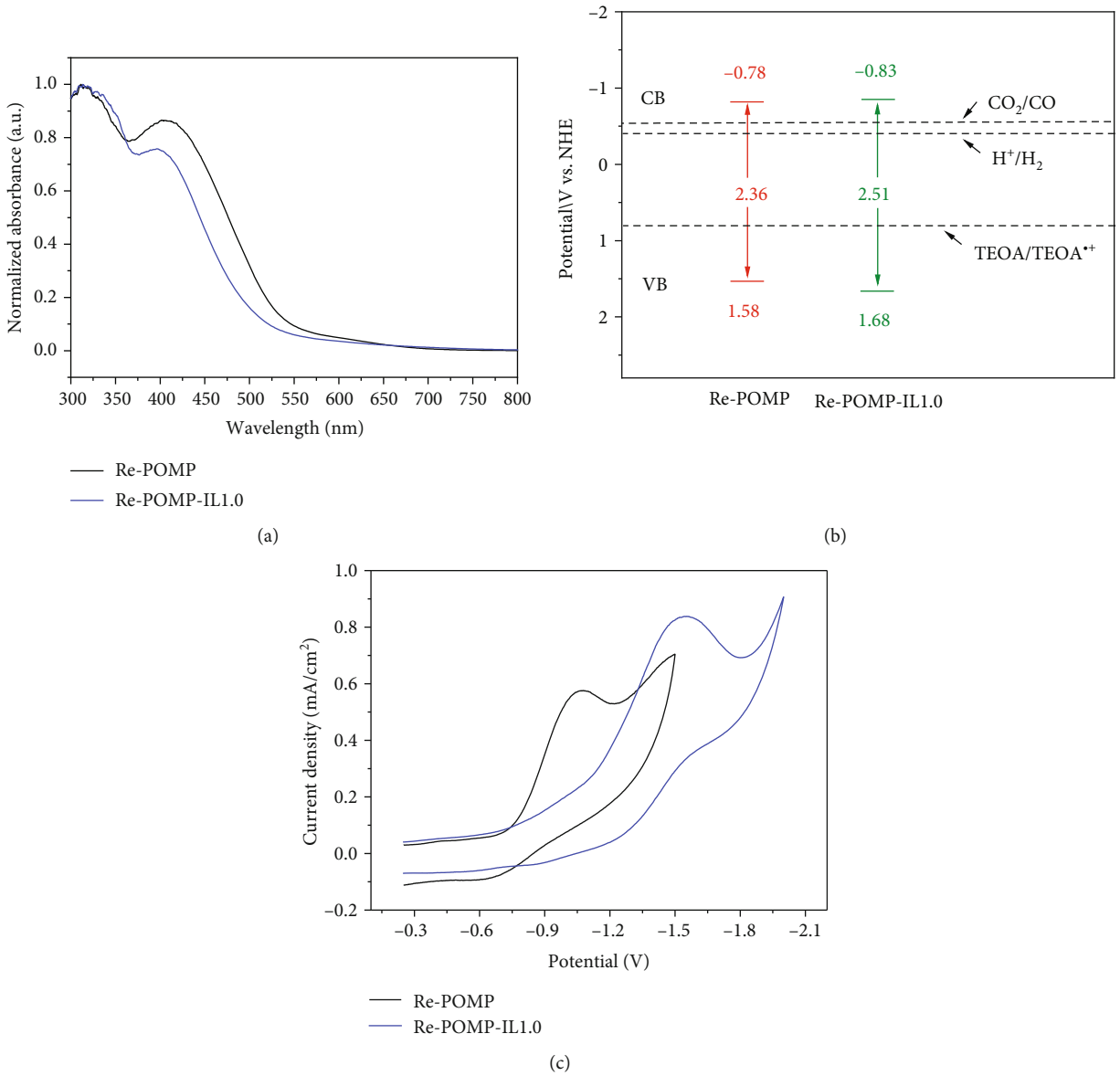

Figure 4: (a) UV/Vis light absorption spectra. (b) CB and VB positions of Re-POMP and Re-POMP-IL1.0. (c) Cyclic voltammograms of Re-POMP and Re-POMP-IL1.0 in acetonitrile with 0.1 M $TBAPF_6$ under air at 50 mV s^{-1}.

being attributed to the electrostatic interaction between IL and CO_2 [39, 40] and the increased Re electron density in Re-POMP-IL1.0.

The optical absorption and band gaps of Re-POMP and Re-POMP-IL1.0 were studied by UV/Vis diffuse reflectance spectra as illustrated in Figure 4(a), in which the good visible-light absorption of polymers was observed. Compared with Re-POMP, Re-POMPIL1.0 shows about 50 nm blue shift in absorption onset, probably being ascribed to the existence of IL reduce the conjugated structures [41]. According to their absorption edges, the optical band gaps of Re-POMP and Re-POMP-IL1.0 were obtained from the Tauc plots, in which the band gap is broadened as the presence of IL unit (Figure S7, see Supplementary Materials). In addition, charge separation behavior was investigated through steady-state time-resolved fluorescence spectroscopy (Figure S8, see Supplementary Materials). Fitting results of the fluorescence attenuation curves showed that lifetimes of 80 and 93 ns were calculated for Re-POMP and Re-POMP-IL1.0 (Table 1), respectively, which are sufficient to enable the polymers to exhibit good charge separation. Specifically, the fluorescence lifetime of the polymer is prolonged after IL addition, meaning that Re-POMP-IL1.0 have more free charge to participate in the photoreaction than Re-POMP.

The semiconductor properties and the electronic band positions were estimated by the Mott-Schottky measurements at frequencies of 500 and 1000 Hz (Figure S9, see Supplementary Materials). Re-POMP and Re-POMP-IL1.0 show characteristics of *n*-type semiconductors in view of the positive slopes of Mott-Schottky plots [42]. For *n*-type semiconductors, the bottoms of the conduction band (CB) positions reflecting the LOMO levels are generally close to

their flat band potentials [21], which are the intersection values on the abscissa obtained by depicting the plots of C^{-2} values relative to applied potentials. As shown in Figure 4(b), LUMO values (bottoms of conduction band) of -0.78 and -0.83 V vs. NHE for Re-POMP and Re-POMP-IL1.0 were measured, respectively. In combination with the band gaps obtained by Tauc plots, the valence band (VB) of 1.58 and 1.68 V vs. NHE for Re-POMP and Re-POMP-IL1.0 were also calculated, respectively. To further have a knowledge of the redox abilities of polymers, cyclic voltammograms of Re-POMP and Re-POMP-IL1.0 were depicted in Figure 4(c). The reduction potentials of Re-POMP and Re-POMP-IL1.0 were observed at -1.07 and -1.55 V vs. Ag/AgCl (-0.87 and -1.35 V vs. NHE), respectively. Obviously, the more negative reduction potentials of Re-POMP and Re-POMP-IL1.0 than $E^0(CO_2/CO)$ (-0.53 V vs. NHE, pH=7 in aqueous solution) [43] make the synthesized polymers exhibit great possibility for photoreduction of CO_2 to CO.

Collectively, the installation of IL into Re-POMP has a little effect on the morphology, while the added IL leads to a decrease in BET surface area so as to affect the CO_2 adsorption capacity, and simultaneously impede the visible-light harvest. On the other hand, the significantly enhanced CO_2 affinity and prolonged lifetime of photogenerated charges are found because of the introduction of IL unit. Upon acquiring these features, the performance of IL-modified Re-based porous material as photocatalyst for CO_2 reduction to CO was evaluated and the decisive factor affecting the CO_2RR was further elucidated.

With Re-POMP-IL1.0 as the photocatalyst, the photocatalytic experiment was firstly carried out under a pure CO_2 atmosphere (1.0 atm, 298 K) in MeCN solution with triethanolamine (TEOA) as the sacrificial agent and 500 W long-arc Xenon lamp ($\lambda \geq 400$ nm) as the light source. As shown in Figure 5(a), CO_2 can be effectively reduced to CO with a TON value of 30.9 and CO selectivity of 95.4%. In fact, the produced CO amount of 40.1 mmol/g Re-POMP-IL1.0 at 12 h is more than those of reported Re(I)-metalated porous polymers [21–25] (Table S1, see Supplementary Materials), probably benefiting from the relatively high Re content and the hierarchical porosity of Re-POMP-IL1.0. No other reduction products such as HCOOH and MeOH were found, and H_2 was detected as a by-product owing to the competitive proton reduction [22]. For comparison, employing Re-POMP as the photocatalyst under the consistent conditions only give TON for CO (TON_{CO}) of 16.1 and selectivity of 69%. These results can clearly demonstrate that IL as a modifier has the ability to enhance the performance of Re(I)-based porous material. In addition, self-polymerization of **2a** was conducted, in which the polymerized ionic liquid named as PIL was obtained and characterized (Figure S10 and S11, see Supplementary Materials). However, physically mixing of Re-POMP and PIL or IL **2a** cannot achieve the comparable activity to that of Re-POMP-IL1.0 and individual PIL or **2a** as the photocatalyst does not work, meaning that the superior properties of IL-modified porous organometallic polymers are the key to enhance the photocatalytic performance.

In addition, it is noteworthy that these synthesized Re-POMPs exhibited even better activity than the homogeneous one, i.e., **1a** (Figure 5(a)), demonstrating the superiority of pore materials which may provide a unique reaction micro-environment and has the ability to increase the CO_2 concentration around the catalytic sites [17, 18]. Particularly, POMP exhibits good photostability and Re-POMP-IL1.0 as the photocatalyst for CO_2 reduction keeps working even if the irradiation time is prolonged to 60 h (Figure 5(b)). At this time, TON_{CO} value is 56 producing CO amount of 73 mmol/g of Re-POMP-IL1.0. Further investigation of the necessity of each component in the catalytic system showed that CO cannot be produced if any of Re-POMP-IL1.0, light source, TEOA, or CO_2 was absent (Table S2 in Supplementary Materials). The isotopic labeling experiment by employing $^{13}CO_2$ for CO_2RR affords ^{13}CO as the major product determined by GC-MS analysis, confirming the CO source originating from CO_2 (Figure S12, see Supplementary Materials).

For CO_2RR, light harvesting, transfer of photogenerated charges as well as CO_2 capture and conversion are key steps [27]. In fact, slightly reduced CO_2 adsorption capacity, shortened optical absorption range, significantly enhanced CO_2 affinity, and prolonged lifetime of photogenerated charges of Re-POMP-IL1.0 relative to Re-POMP were observed in this study (see Figures 3(c) and 4(a), Table 1, and Figure S8). The better catalytic performance of Re-POMP-IL1.0 than Re-POMP suggests that the processes of interaction with CO_2 and separation of photogenerated charges may be closer factors than CO_2 uptake amount and optical property for POMPs catalyzed CO_2RR.

In view that the amount of IL in polymer has an effect on the properties, which may affect its photocatalytic activity, Re-POMP-IL0.4 and Re-POMP-IL1.5 were prepared by adjusting the amount of added **2a** in copolymerization using the same synthetic method with Re-POMP-IL1.0. Through ICP-OES, Re contents in Re-POMP-IL0.4 and Re-POMP-IL1.5 were measured as 29.3 and 22.6 wt%, respectively. The N_2 adsorption/desorption isotherms, pore size distributions, porosity properties, CO_2 uptake capacities, and excited-state lifetimes of Re-POMP-IL0.4 and Re-POMP-IL1.5 were measured in comparison with those of Re-POMP and Re-POMP-IL1.0 in Figure S13 and Table S3 (see Supplementary Materials). Re-POMP-IL1.5 exhibits much lower surface area than other POMPs, being attributed to the significantly reduced meso- and micropores probably because of the blocking of intrinsic pores by more IL [38]. The higher CO_2 uptake amounts of Re-POMP-IL0.4 than Re-POMP further highlight the positive effect of IL on CO_2 absorption, while the reduced CO_2 uptake amounts of Re-POMP-IL1.0 and Re-POMP-IL1.5 than those of Re-POMP could be probably due to their obviously reduced BET surface area and pore volume. Accompanying with the introduction of IL, the gradually increasing Q_{st} values in the order of Re-POMP-IL1.0>Re-POMP-IL0.4>Re-POMP were observed, suggesting the enhanced CO_2 capture with more IL installed. On the other hand, CO_2 absorption behavior is also affected by porous properties; thus, a slight reduced

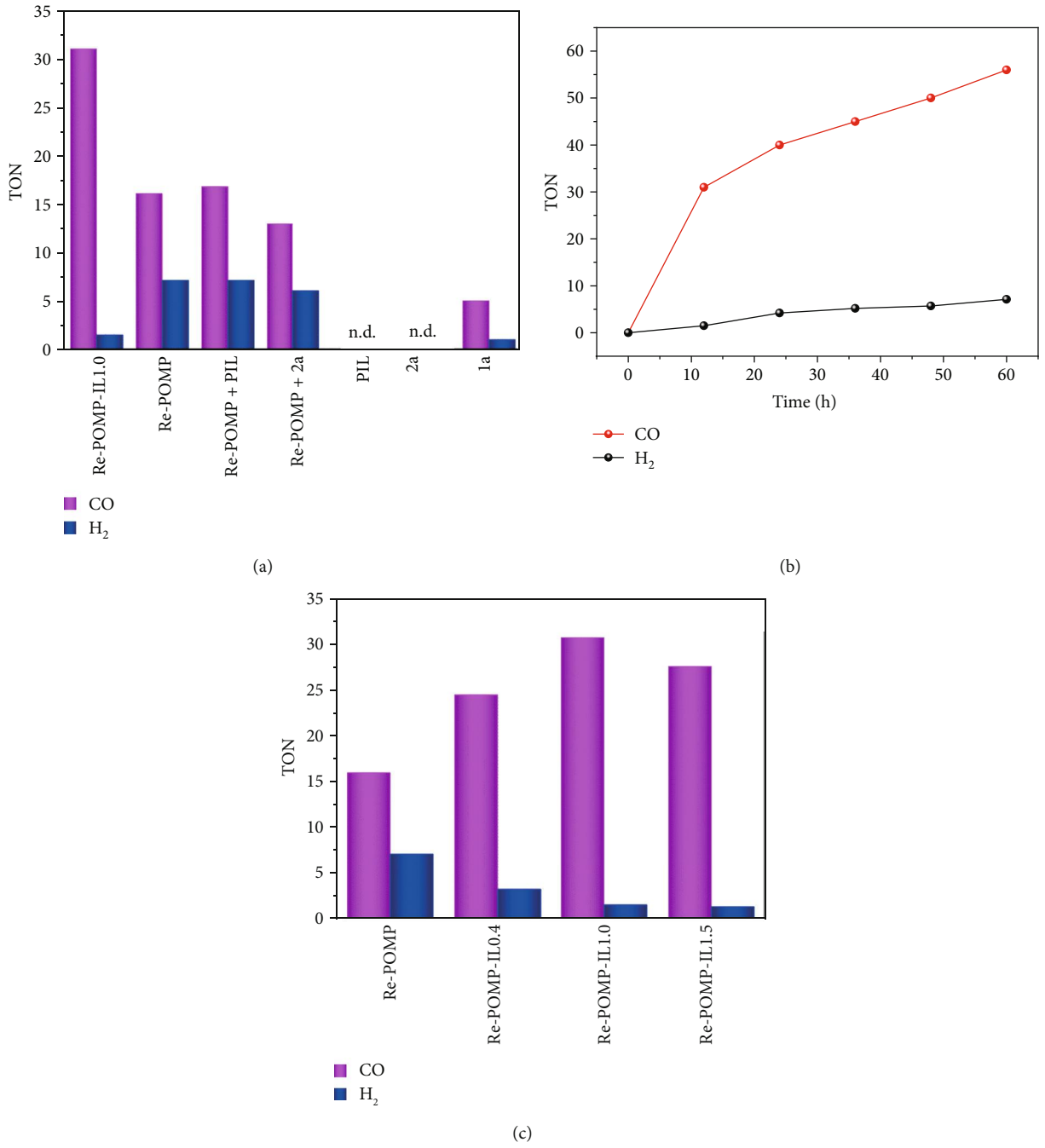

FIGURE 5: (a) Photocatalytic tests. (b) CO and H_2 production curves over Re-POMP-IL1.0. (c) TON of CO and H_2 with POMPs as the photocatalysts.

Q_{st} value of Re-POMP-IL1.5 compared with Re-POMP-IL1.0 may be attributed to its significantly reduced meso- and micropores. The low to moderate Q_{st} values of POMPs allow reversible CO_2 absorption and relatively easy CO_2 desorption, indicating major physical adsorption rather than chemical adsorption of POMPs for CO_2 uptake was performed [38, 44]. Moreover, the continually prolonged excited-state lifetimes of POMPs accompanied with the increase of added IL amount were discovered.

Then, Re-POMP-IL0.4 and Re-POMP-IL1.5 were applied to the photocatalytic CO_2 reduction and both of them exhibits higher activity and CO selectivity than Re-POMP (Figure 5(c)), further illustrating the promoting effect on photocatalytic performance by chemically introducing IL into polymer and simultaneously proving the rationality of the design. In addition, the amount of IL in polymer also has an influence on the activity. Increased TON_{CO} and selectivity of CO were found when advancing the amount of **2a** from 0 to 1.0 equivalent relative to **1a**, probably profiting

from the increased IL in polymer can reduce its energy consumption for CO_2 capture and simultaneously lead to the prolonged excited-state lifetime. However, continuing to increase the amount of **2a** to 1.5 equivalent relative to **1a**, the produced CO began to decrease even though Re-POMP-IL1.5 owns the longest excited-state lifetime among these polymers. On the other hand, the enhanced photocatalytic activity in the order of Re-POMP<Re-POMP-IL0.4<Re-POMP-IL1.5<Re-POMP-IL1.0 was observed (Figure 5(c), Table S3), being consistent with their Q_{st} values. These results further elucidate the important effect of CO_2 affinity on CO_2RR using POMPs as the photocatalysts. This finding is different from the previous work, in which the high CO_2 adsorption capacity, broadened optical absorption, and/or facile charge separation are always highlighted [21, 23, 25].

3. Discussion

In conclusion, the IL-modified Re-based porous organometallic polymers (Re-POMP-IL) have been designed and developed as effective photocatalysts for CO_2 reduction to CO. Specifically, the installation of IL (3-ethyl-1-vinyl-1*H*-imidazol-3-ium bromide used in this work) can obviously enhance the photocatalytic activity and CO selectivity. Re-POMP-IL can be obtained through radical copolymerization, which is simple and scalable. Characteristics on pore features, optical properties, redox abilities, and excited-state lifetimes of Re-POMP-IL demonstrated that they have high CO_2 uptake capacities, visible-light absorption, suitable redox potential, and long enough excited-state lifetimes for CO_2 reduction. Catalytic activity tests showed that Re-POMP-IL behaves better than Re-POMP in promoting CO_2 to selectively produce CO, and the competitive H_2 evolution can be effectively suppressed with CO selectivity up to 95.5%. Investigation on the effect of IL content on the catalytic performance of POMPs shows that Re-POMP-IL1.0 with the largest CO_2 isosteric heat of adsorption exhibits the best catalytic performance, emphasizing the important role of CO_2 affinity for POMPs catalyzed CO_2RR. In a word, these results demonstrate the feasibility of using IL as a regulator to develop efficient and selective photocatalyst for CO_2 reduction.

4. Materials and Methods

4.1. Synthesis of [(5,5′-divinyl-2,2′-bipyridine)Re(CO)$_3$Cl] (1a). For the synthesis of **1a**, 5,5′-divinyl-2,2′-bipyridine as ligand was obtained through the cross-coupling of potassium vinyltrifluoroborate with 5,5′-dibromo-2,2′-bipyridine [45] and then coordinated with $Re(CO)_5Cl$. Detailed procedure is listed as follows: to a 250 mL three-necked bottle, 5,5′-dibromo-2,2′-bipyridine (0.9420 g, 3 mmol), potassium vinyltrifluoroborate (1.4997 g, 11.2 mmol), $Pd(OAc)_2$ (0.0013 g, 0.06 mmol), PPh_3 (0.0042 g, 0.16 mmol), and Cs_2CO_3 (2.7367 g, 8.4 mmol) were sequentially added, and then THF (48 mL) and H_2O (2 mL) were injected under N_2 atmosphere. The obtained mixture was refluxed for 16 h. When the reaction finished, the resultant solution was cooled to room temperature and water (50 mL) was added. Then, the mixture was extracted with ethyl acetate (30 mL × 3), and the resulting organic layers were combined. After dried over anhydrous Na_2SO_4, the organic extracts were concentrated under vacuum and the residue was purified by chromatography on silica gel with petroleum ether and ethyl acetate (5/1-2/1) as eluents to give 5,5′-divinyl-2,2′-bipyridine.

Then, 5,5′-divinyl-2,2′-bipyridine (0.2083 g, 1 mmol) and $Re(CO)_5Cl$ (0.3617 g, 1 mmol) were mixed in a 250 mL three-necked bottle. After this, toluene (100 mL) was injected under N_2 atmosphere. The reaction was carried out under reflux for 16 h. When finished, the resulting mixture was cooled to room temperature, and the yellow precipitate was filtered off, washed with toluene, and dried under vacuum to give **1a**.

5,5'-Divinyl-2,2'-bipyridine [36]: white solid (0.3064 g, 42% yield); m.p.: 79-80°C. IR (neat, KBr): 3091, 3051, 3007, 2992, 1972, 1802, 1626, 1588, 1467, 1361, 1054, 1019, 898, and 850 cm^{-1}. ^1H NMR (400 MHz, $CDCl_3$) δ 8.67 (s, 2H), 8.38 (d, J = 8.1 Hz, 2H), 7.88 (d, J = 8.3 Hz, 2H), 6.77 (dd, J = 17.6, 11.0 Hz, 2H), 3.90 (d, J = 17.6 Hz, 2H), 3.43 (d, J = 11.0 Hz, 2H) ppm. ^{13}C NMR (101 MHz, $CDCl_3$) δ 134.99, 147.77, 133.43, 133.28, 132.94, 120.73, and 116.31 ppm. HRMS (ESI): m/z calcd for $C_{14}H_{13}N_2H$ $[M+H]^+$: 209.1068; found: 209.1076.

1a: yellow solid (0.4295 g, 84% yield). IR (neat, KBr): 3101, 3070, 3040, 2018, 1914, 1877, 1480, 1379, 1251, 918, and 860 cm^{-1}. ^1H NMR (400 MHz, $CDCl_3$) δ 8.98 (s, 2H), 8.07 (dt, J = 8.4, 3.1 Hz, 4H), 6.78 (dd, J = 17.6, 11.0 Hz, 2H), 6.03 (d, J = 17.6 Hz, 2H), 3.68 (d, J = 11.0 Hz, 2H) ppm. HRMS (ESI): m/z calcd for $C_{17}H_{12}N_2O_3Re$ $[M\text{-}Cl]^+$: 479.0400; found: 479.0391.

4.2. Synthesis of 3-Ethyl-1-Vinyl-1H-Imidazol-3-Ium Bromide (2a) [46]. To a 50 mL Schlenk tube, 1-vinyl-1*H*-imidazole (4.9873 g, 53 mmol) and bromoethane (6.5400 g, 60 mmol) were added. The mixture was refluxed at 70°C for 3 h and then cooled to room temperature to give the white solid. The desired **2a** was obtained after drying the white solid under vacuum at 70°C for overnight.

2a [46]: white solid (10.9509 g, 98% yield). IR (neat, KBr): 3133, 3076, 2991, 1655, 1573, 1550, 1170, 961, and 926 cm^{-1}. ^1H NMR (400 MHz, DMSO-d_6) δ 9.61 (s, 1H), 8.23 (d, J = 1.5 Hz, 1H), 7.98 (s, 1H), 7.32 (dd, J = 15.6, 8.8 Hz, 1H), 5.98 (dd, J = 15.6, 2.3 Hz, 1H), 5.41 (dd, J = 8.7, 2.3 Hz, 1H), 4.24 (q, J = 7.3 Hz, 2H), 1.45 (t, J = 7.3 Hz, 3H) ppm. ^{13}C NMR (101 MHz, D_2O) δ 134.07, 128.26, 122.55, 119.40, 109.20, 45.22, and 14.34 ppm.

4.3. Synthesis of Re-POMP. **1a** (200 mg, 0.39 mmol), AIBN (10 mg, 0.06 mmol), and DMF (7 mL) were added to a 25 mL autoclave. Then, the autoclave was sealed and heated at 100°C for 24 h. When finished, the autoclave was cooled to room temperature and the resulting mixture was transferred to a 50 mL conical flask, followed by adding 20 mL ethanol to soak overnight. Then, the obtained mixture was filtered and washed with ethanol until the filtrate was colorless. After the filter cake was dried under vacuum at 70°C for overnight, the yellow solid (185.7 mg) was obtained and named as Re-POMP.

4.4. Synthesis of Re-POMP-IL. Take the synthesis of Re-POMP-IL1.0 as an example, **1a** (200 mg, 0.39 mmol), **2a** (78.8 mg, 0.39 mmol), AIBN (10 mg, 0.06 mmol), and DMF (7 mL) were added to a 25 mL autoclave. Then, the autoclave was heated at 100°C for 24 h. When finished, the autoclave was cooled to room temperature and the resulting mixture was transferred to a 50 mL conical flask, followed by adding 20 mL ethanol to soak overnight. Then, the obtained mixture was filtered and washed with ethanol until the filtrate was colorless. After the filter cake was dried under vacuum at 70°C for overnight, the yellow solid (268.3 mg) was obtained and named as Re-POMP-IL1.0.

For the synthesis of Re-POMP-IL0.4 and Re-POMP-IL1.5, their synthetic procedures are similar to that of Re-POMP-IL1.0, except that the amount of **2a** added was adjusted to 0.16 mmol and 0.59 mmol, respectively.

4.5. Synthesis of PIL. **2a** (505 mg, 2.5 mmol), AIBN (24.6 mg, 0.15 mmol), and ethanol (5 mL) were added to a 50 mL Schlenk flask under Ar atmosphere. Then, the reaction was conducted at 80°C for 16 h. When finished, the resultant mixture was cooled to room temperature, followed by adding 20 mL ethanol to soak overnight. Then, the obtained mixture was filtered and washed with ethanol (5 × 20 mL). After the filter cake was dried under vacuum at 70°C for overnight, PIL (420.2 mg) was obtained as white solid.

4.6. General Procedure for Photocatalytic CO_2 Reduction. To a 25 mL Schlenk tube, photocatalyst (1 mg), TEOA (1.12 g, 1 mL) and MeCN (3 mL) were successively added. Then, the reaction mixture was sonicated to allow the polymer to disperse evenly in the whole solution. Air in the Schlenk tube was replaced by CO_2 through the freeze-pump-thaw method. Then, the reaction tube was sealed and placed under a 500 W long-arc Xenon lamp ($\lambda \geq 400$ nm) for 12 h at room temperature. The light source was cooled by flowing cooling water before irradiating the reaction tube and the number of moles of photons absorbed by the photocatalyst was measured as 1.4×10^{-8} einstein/s (see Supplementary Materials). After the reaction, partial gaseous products (1 mL) were taken from the tube using a syringe and then analyzed by gas chromatography with a TCD detector.

Conflicts of Interest

The authors declare no conflict of interest.

Acknowledgments

This work was financially supported by the National Natural Science Foundation of China (21672119, 21975135), China Postdoctoral Science Foundation (2018M641624), National Key Research and Development Program (2016YFA0602900), and the Ph.D. Candidate Research Innovation Fund of the College of Chemistry Nankai University. We also appreciate the support from Prof. Tong Bu Lu, Dr. Song Guo, and Ping Wang (Tianjin University of Technology) in photoluminescence lifetime measurement.

Supplementary Materials

Figure S1: ^{1}H and ^{13}C NMR of 5,5′-divinyl-2,2′-bipyridine. Figure S2: ^{1}H NMR of [(5,5′-divinyl-2,2′-bipyridine)Re(-CO)^{3}Cl] (**1a**). Figure S3: ^{1}H and ^{13}C NMR of 3-ethyl-1-vinyl-1*H*-imidazol-3-ium bromide (**2a**). Figure S4: SEM images of (a) Re-POMP and (b) Re-POMP-IL1.0; TEM images of (c) Re-POMP and (d) Re-POMP-IL1.0. Figure S5: TGA curves of Re-POMP and Re-POMP-IL1.0 in nitrogen. Figure S6: powder X-ray diffraction (PXRD) of Re-POMP-IL1.0. Figure S7: Tauc plots of (a) Re-POMP and (b) Re-POMP-IL1.0. Figure S8: fluorescence decay curves of Re-POMP and Re-POMP-IL1.0 in solid/air at room temperature. Figure S9: Mott-Schottky plots of (a) Re-POMP and (b) Re-POMP-IL1.0 in 0.1 M $TBABF_6$ acetonitrile solution at 500 and 1000 Hz. Figure S10: FT-IR spectra of PIL and **2a**. Figure S11: SEM image of PIL. Figure S12: GC-MS spectrum of photogenerated ^{13}CO under $^{13}CO_2$ atmosphere with Re-POMP-IL1.0 as the photocatalyst. Figure S13: (a) nitrogen sorption isotherms collected at 77 K. (b) Pore size distributions calculated by NLDFT. Table S1: comparison of Re content and the produced CO amount of Re-POMP-IL1.0 with the reported Re-based porous polymers and other porous materials. Table S2: control experiments of photoreduction of CO_2[a]. Table S3: porosity properties, CO_2 uptake capacities, and lifetimes of excited states of the polymers and photocatalytic results of the polymers. *(Supplementary Materials)*

References

[1] J. Ran, M. Jaroniec, and S. Z. Qiao, "Cocatalysts in semiconductor-based photocatalytic CO_2 reduction: achievements, challenges, and opportunities," *Advanced Materials*, vol. 30, no. 7, article 1704649, 2018.

[2] K. E. Dalle, J. Warnan, J. J. Leung, B. Reuillard, I. S. Karmel, and E. Reisner, "Electro- and solar-driven fuel synthesis with first row transition metal complexes," *Chemical Reviews*, vol. 119, no. 4, pp. 2752–2875, 2019.

[3] S. Berardi, S. Drouet, L. Francàs et al., "Molecular artificial photosynthesis," *Chemical Society Reviews*, vol. 43, no. 22, pp. 7501–7519, 2014.

[4] J. L. White, M. F. Baruch, J. E. Pander et al., "Light-driven heterogeneous reduction of carbon dioxide: photocatalysts and photoelectrodes," *Chemical Reviews*, vol. 115, no. 23, pp. 12888–12935, 2015.

[5] Y. Zhao and Z. Liu, "Recent advances in photocatalytic CO_2 reduction using earth-abundant metal complexes-derived photocatalysts," *Chinese Journal of Chemistry*, vol. 36, no. 5, pp. 455–460, 2018.

[6] J. Wu, R. M. Yadav, M. Liu et al., "Achieving highly efficient, selective, and stable CO_2 reduction on nitrogen-doped carbon nanotubes," *ACS Nano*, vol. 9, no. 5, pp. 5364–5371, 2015.

[7] D. M. Koshy, S. Chen, D. U. Lee et al., "Understanding the origin of highly selective CO_2 electroreduction to CO on Ni,N-doped carbon catalysts," *Angewandte Chemie International Edition*, vol. 59, no. 10, pp. 4043–4050, 2020.

[8] Y. Kuramochi, O. Ishitani, and H. Ishida, "Reaction mechanisms of catalytic photochemical CO_2 reduction using Re(I)

and Ru(II) complexes," *Coordination Chemistry Reviews*, vol. 373, pp. 333–356, 2018.

[9] J. Hawecker, J.-M. Lehn, and R. Ziessel, "Efficient photochemical reduction of CO_2 to CO by visible light irradiation of systems containing $Re(bipy)(CO)_3X$ or $Ru(bipy)_3^{2+}$–Co^{2+}combinations as homogeneous catalysts," *Journal of the Chemical Society, Chemical Communications*, vol. 1983, no. 9, pp. 536–538, 1983.

[10] J. Hawecker, J.-M. Lehn, and R. Ziessel, "Photochemical and electrochemical reduction of carbon dioxide to carbon monoxide mediated by (2,2′-bipyridine)tricarbonylchlororhenium(I) and related complexes as homogeneous catalysts," *Helvetica Chimica Acta*, vol. 69, no. 8, pp. 1990–2012, 1986.

[11] A. J. Huckaba, E. A. Sharpe, and J. H. Delcamp, "Photocatalytic reduction of CO_2 with Re-Pyridyl-NHCs," *Inorganic Chemistry*, vol. 55, no. 2, pp. 682–690, 2016.

[12] H. Takeda, K. Koike, H. Inoue, and O. Ishitani, "Development of an efficient photocatalytic system for CO_2 reduction using rhenium(I) complexes based on mechanistic studies," *Journal of the American Chemical Society*, vol. 130, no. 6, pp. 2023–2031, 2008.

[13] T. Morimoto, T. Nakajima, S. Sawa, R. Nakanishi, D. Imori, and O. Ishitani, "CO_2 capture by a rhenium(I) complex with the aid of triethanolamine," *Journal of the American Chemical Society*, vol. 135, no. 45, pp. 16825–16828, 2013.

[14] D. R. Whang, D. H. Apaydin, S. Y. Park, and N. S. Sariciftci, "An electron-reservoir Re(I) complex for enhanced efficiency for reduction of CO_2 to CO," *Journal of Catalysis*, vol. 363, pp. 191–196, 2018.

[15] P. L. Cheung, S. C. Kapper, T. Zeng, M. E. Thompson, and C. P. Kubiak, "Improving photocatalysis for the reduction of CO_2 through non-covalent supramolecular assembly," *Journal of the American Chemical Society*, vol. 141, no. 38, pp. 14961–14965, 2019.

[16] K.-H. Chen, N. Wang, Z.-W. Yang, S. M. Xia, and L. N. He, "Tuning of ionic second coordination sphere in evolved rhenium catalyst for efficient visible-light-driven CO_2 reduction," *ChemSusChem*, 2020.

[17] Q. Sun, Z. Dai, X. Meng, and F. S. Xiao, "Porous polymer catalysts with hierarchical structures," *Chemical Society Reviews*, vol. 44, no. 17, pp. 6018–6034, 2015.

[18] Q. Sun, Z. Dai, X. Meng, L. Wang, and F.-S. Xiao, "Task-specific design of porous polymer heterogeneous catalysts beyond homogeneous counterparts," *ACS Catalysis*, vol. 5, no. 8, pp. 4556–4567, 2015.

[19] H. Bildirir, V. G. Gregoriou, A. Avgeropoulos, U. Scherf, and C. L. Chochos, "Porous organic polymers as emerging new materials for organic photovoltaic applications: current status and future challenges," *Materials Horizons*, vol. 4, no. 4, pp. 546–556, 2017.

[20] T. Zhang, G. Xing, W. Chen, and L. Chen, "Porous organic polymers: a promising platform for efficient photocatalysis," *Materials Chemistry Frontiers*, vol. 4, no. 2, pp. 332–353, 2020.

[21] H.-P. Liang, A. Acharjya, D. A. Anito et al., "Rhenium-metalated polypyridine-based porous polycarbazoles for visible-light CO_2 photoreduction," *ACS Catalysis*, vol. 9, no. 5, pp. 3959–3968, 2019.

[22] W. Liang, T. L. Church, S. Zheng, C. Zhou, B. S. Haynes, and D. M. D'Alessandro, "Site isolation leads to stable photocatalytic reduction of CO_2 over a rhenium-based catalyst," *Chemistry A European Journal*, vol. 21, no. 51, pp. 18576–18579, 2015.

[23] R. Xu, X.-S. Wang, H. Zhao, H. Lin, Y. B. Huang, and R. Cao, "Rhenium-modified porous covalent triazine framework for highly efficient photocatalytic carbon dioxide reduction in a solid–gas system," *Catalysis Science & Technology*, vol. 8, no. 8, pp. 2224–2230, 2018.

[24] Z. Fu, X. Wang, A. M. Gardner et al., "A stable covalent organic framework for photocatalytic carbon dioxide reduction," *Chemical Science*, vol. 11, no. 2, pp. 543–550, 2020.

[25] S. Yang, W. Hu, X. Zhang et al., "2D covalent organic frameworks as intrinsic photocatalysts for visible light-driven CO_2 reduction," *Journal of the American Chemical Society*, vol. 140, no. 44, pp. 14614–14618, 2018.

[26] Y. Shen, Q. Zheng, H. Zhu, and T. Tu, "Hierarchical porous organometallic polymers fabricated by direct knitting: recyclable single-site catalysts with enhanced activity," *Advanced Materials*, vol. 32, no. 6, article 1905950, 2019.

[27] R. Li, W. Zhang, and K. Zhou, "Metal-organic-framework-based catalysts for photoreduction of CO_2," *Advanced Materials*, vol. 30, no. 35, article 1705512, 2018.

[28] S. Zeng, X. Zhang, L. Bai et al., "Ionic-liquid-based CO_2 capture systems: structure, interaction and process," *Chemical Reviews*, vol. 117, no. 14, pp. 9625–9673, 2017.

[29] S. Wang and X. Wang, "Imidazolium ionic liquids, imidazolylidene heterocyclic carbenes, and zeolitic imidazolate frameworks for CO_2 capture and photochemical reduction," *Angewandte Chemie International Edition*, vol. 55, no. 7, pp. 2308–2320, 2016.

[30] F.-F. Chen, K. Huang, Y. Zhou et al., "Multi-molar absorption of CO_2 by the activation of carboxylate groups in amino acid ionic liquids," *Angewandte Chemie International Edition*, vol. 55, no. 25, pp. 7166–7170, 2016.

[31] C. Wu, H. Zhang, B. Yu et al., "Lactate-based ionic liquid catalyzed reductive amination/cyclization of keto acids under mild conditions: a metal-free route to synthesize lactams," *ACS Catalysis*, vol. 7, no. 11, pp. 7772–7776, 2017.

[32] J. Hu, J. Ma, Q. Zhu, Z. Zhang, C. Wu, and B. Han, "Transformation of atmospheric CO_2 catalyzed by protic ionic liquids: efficient synthesis of 2-oxazolidinones," *Angewandte Chemie International Edition*, vol. 54, no. 18, pp. 5399–5403, 2015.

[33] Y. Huang, G. Cui, Y. Zhao et al., "Preorganization and cooperation for highly efficient and reversible capture of low-concentration CO_2 by ionic liquids," *Angewandte Chemie International Edition*, vol. 56, no. 43, pp. 13293–13297, 2017.

[34] J. Lin, Z. Ding, Y. Hou, and X. Wang, "Ionic liquid Co-catalyzed artificial photosynthesis of CO," *Scientific Reports*, vol. 3, no. 1, p. 1056, 2013.

[35] Y. Chen, G. Ji, S. Guo et al., "Visible-light-driven conversion of CO_2 from air to CO using an ionic liquid and a conjugated polymer," *Green Chemistry*, vol. 19, no. 24, pp. 5777–5781, 2017.

[36] Z. Dai, Q. Sun, X. Liu et al., "A hierarchical bipyridine-constructed framework for highly efficient carbon dioxide capture and catalytic conversion,," *ChemSusChem*, vol. 10, no. 6, pp. 1186–1192, 2017.

[37] K. S. W. Sing, D. H. Everett, R. A. W. Haul et al., "Reporting physisorption data for gas/solid systems with special reference to the determination of surface area and porosity (Provisional)," *Pure and Applied Chemistry*, vol. 54, no. 11, pp. 2201–2218, 1982.

[38] C. Cui, R. Sa, Z. Hong, H. Zhong, and R. Wang, "Ionic liquid-modified click-based porous organic polymers for controlling capture and catalytic conversion of CO_2," *ChemSusChem*, vol. 13, no. 1, pp. 180–187, 2020.

[39] Y. F. Chen, A. Nalaparaju, M. Eddaoudi, and J. W. Jiang, "CO_2 adsorption in mono-, di- and trivalent cation-exchanged metal–organic frameworks: a molecular simulation study," *Langmuir*, vol. 28, no. 8, pp. 3903–3910, 2012.

[40] H. J. Park and M. P. Suh, "Enhanced isosteric heat, selectivity, and uptake capacity of CO_2 adsorption in a metal-organic framework by impregnated metal ions," *Chemical Science*, vol. 4, no. 2, pp. 685–690, 2013.

[41] D. Chen, C. Cui, N. Tong, H. Zhou, X. Wang, and R. Wang, "Water-soluble and low-toxic ionic polymer dots as invisible security ink for multiStage information encryption," *ACS Applied Materials & Interfaces*, vol. 11, no. 1, pp. 1480–1486, 2019.

[42] Z. Vlčková Živcová, O. Frank, S. Drijkoningen, K. Haenen, V. Mortet, and L. Kavan, "n-type phosphorus-doped nanocrystalline diamond: electrochemical and in situ raman spectroelectrochemical study," *RSC Advances*, vol. 6, no. 56, pp. 51387–51393, 2016.

[43] E. E. Benson, C. P. Kubiak, A. J. Sathrum, and J. M. Smieja, "Electrocatalytic and homogeneous approaches to conversion of CO_2 to liquid fuels," *Chemical Society Reviews*, vol. 38, no. 1, pp. 89–99, 2009.

[44] C. F. Martín, E. Stöckel, R. Clowes et al., "Hypercrosslinked organic polymer networks as potential adsorbents for pre-combustion CO_2 capture," *Journal of Materials Chemistry*, vol. 21, no. 14, pp. 5475–5483, 2011.

[45] H.-J. Nie, J. Yao, and Y.-W. Zhong, "Synthesis of vinyl-substituted polypyridyl ligands through Suzuki–Miyaura cross-coupling of potassium vinyltrifluoroborate with bromopolypyridines," *The Journal of Organic Chemistry*, vol. 76, no. 11, pp. 4771–4775, 2011.

[46] J. L. Hickey, R. A. Ruhayel, P. J. Barnard, M. V. Baker, S. J. Berners-Price, and A. Filipovska, "Mitochondria-targeted chemotherapeutics: the rational design of gold(I) N-heterocyclic carbene complexes that are selectively toxic to cancer cells and target protein selenols in preference to thiols," *Journal of the American Chemical Society*, vol. 130, no. 38, pp. 12570-12571, 2008.